Electrical Power and Energy Systems 113 (2019) 618–633

Contents lists available at ScienceDirect

Electrical Power and Energy Systems

journal homepage: www.elsevier.com/locate/ijepes

A system optimization method for mitigating three-phase imbalance in distribution network

X.J. Zeng[a], H.F. Zhai[b], M.X. Wang[a,*], M. Yang[a], M.Q. Wang[a]

[a] Key Laboratory of Power System Intelligent Dispatch and Control (Shandong University), Ministry of Education, Jinan 250061, China
[b] Electric Power Research Institute of China Southern Power Grid, Guangzhou 510663, Guangdong Province, China

ARTICLE INFO

Keywords:
Three-phase imbalance
Three-phase four-wire
Joint optimization model
Linearization techniques
Mixed-integer linear programming

ABSTRACT

Three-phase imbalance is a common phenomenon in three-phase four-wire distribution network systems (DNSs), which may cause power quality deterioration, increase power losses, and can even damage appliances as well. The situation is becoming even worse because of the increasing integration of the distributed generations (DGs) and storage-capable loads into DNSs. In this paper, a joint optimization model based on the Y-connected and Δ-connected static reactive power compensation devices are proposed to mitigate the three-phase imbalance and minimize the active power losses in DNSs. The model is formulated to optimize the operation of all the devices in order to mitigate the imbalance of the whole DNS rather than a single feeder or a particular area. Meanwhile, the current imbalance of the transformer and the voltage imbalance of all three-phase nodes are simultaneously considered in the model according to the practical requirements. Several linearization techniques are applied to simplify the computation and accelerate the solving speed. These techniques convert the non-linear and non-convex model into a mixed-integer linear programming model, which can be effectively solved by off-the-shelf solvers. The effectiveness and scalability of the proposed method are verified by the test results obtained from the modified IEEE 34 and IEEE 123 test systems.

1. Nomenclature

In this section, bold symbols represent three-phase vectors unless otherwise specified. The subscript t denotes the tth period, and node f is the root node. Moreover, if one node connects with a single-phase load, the power, voltage and current of the rest phases are defined as zero directly.

B	set of all branches
E	set of nodes connected with ESSs
F	set of nodes connected with substations
G	set of nodes connected with DGs
L	set of nodes connected with loads
M	set of nodes connected with TPLRDs
N	set of all nodes
T	set of time periods (e.g., 24 h)
$\boldsymbol{S}_{ij,t}$	vector of the apparent power from node i to node j
$\boldsymbol{P}_{ij,t}$, $\boldsymbol{Q}_{ij,t}$	vectors of the active and reactive power flow from node i to node j
$\boldsymbol{P}_{ki,t}$, $\boldsymbol{Q}_{ki,t}$	vectors of the active and reactive power injected from upstream node k to node i
$\boldsymbol{P}_{f,t}$, $\boldsymbol{Q}_{f,t}$	vectors of active and reactive power injected from the substation located at node i
$\boldsymbol{P}_{e,t}$, $\boldsymbol{Q}_{e,t}$	vectors of the active and reactive power generated by EES
$\boldsymbol{P}_{g,t}$, $\boldsymbol{Q}_{g,t}$	vectors of three-phase active and reactive power injected from DG
$\boldsymbol{P}^{c}_{e,t}$, $\boldsymbol{Q}^{c}_{e,t}$/$\boldsymbol{P}^{d}_{e,t}$, $\boldsymbol{Q}^{d}_{e,t}$	vectors of the active and reactive charging/discharging power of ESS
$\tilde{\boldsymbol{P}}_{m,t}$, $\tilde{\boldsymbol{Q}}_{m,t}$	vectors of the equivalent active and reactive power supplied by TPLDR
$\rho^{c}_{e,t}$, $\rho^{d}_{e,t}$	binary variables, represent the charging and discharging state
η^{c}, η^{d}	charging and discharging efficiency of ESS
$SOC_{e,t}$	state of charge of ESS
$VUF_{i,t}$	voltage imbalance degree at node i
U^{ref}_{f}	square of the root node voltage
$I^{+}_{f,t}$, $I^{-}_{f,t}$	positive and negative sequence current of the root node
$CUF_{f,t}$	current imbalance degree of root node
ε	$e^{j2\pi/3}$
V^{min}_{i}, V^{max}_{i}	lower and upper limits of voltage magnitude at node i
Q^{Δ}_{min}, Q^{Δ}_{max}	lower and upper limits of reactive power compensation capacity by Δ-connected SVCs
Q^{Y}_{min}, Q^{Y}_{max}	lower and upper limits of reactive power compensation capacity by Y-connected SVCs
$U^{ave}_{i,t}$	mean of squared voltage magnitude of three phases
δ	conservative constraint coefficient for current imbalance

* Corresponding author.
E-mail address: wangmx@sdu.edu.cn (M.X. Wang).

https://doi.org/10.1016/j.ijepes.2019.05.038
Received 22 December 2018; Received in revised form 9 April 2019; Accepted 14 May 2019
Available online 11 June 2019
0142-0615/

$LF_{f,t}^{load}$	three-phase active/reactive power imbalance rate flowing through the distribution transformer

2. Introduction

Three-phase four-wire wiring is widely applied in distribution network systems (DNSs), which usually have closed-loop structures but are typically operated in open loops [1]. In DNSs, there are a large number of scattered power loads, and most of them are single-phase loads or single- and three-phase mixed loads. These loads are unevenly distributed in feeders, resulting in three-phase voltage and current imbalance in DNSs. Particularly, when additional renewable distributed generations (DGs) such as photovoltaics (PVs) and wind generators (WGs), energy storage systems (ESSs) and new storage-capable loads such as electric vehicles (EVs) are connected into DNSs, the three-phase imbalance would become even worse because of the intermittency of DGs and the reverse power flow [2,3].

In three-phase four-wire DNSs, unbalanced voltage and current would lead to severe operational issues. The current imbalance would increase the losses of distribution lines and result in more harmonic currents that would adversely affect the power quality. Moreover, the distribution transformers are usually designed for three-phase balanced loads, and their capacity would be limited by the heaviest load phase. When unbalanced current flows through a distribution transformer, it will lead to an increase in the temperature of the heaviest load phase and then limit the transmission capability of the transformer [4]. In addition, the current imbalance can cause negative and zero sequence components in lines, which may mis-trigger protections based on the negative and zero sequence components [5]. The voltage imbalance can significantly affect the operation of induction motors. It may cause extremely high winding temperature, which would accelerate the aging of the insulation materials and significantly shorten the service life of the machine [6]. Meanwhile, the voltage imbalance may result in torque fluctuation that will reduce the efficiency of the motor and even damage the device [7]. Therefore, it is necessary to maintain three-phase load balance in DNSs, which can not only improve the power quality, security and reliability, but also enhance the utility's competitive ability in the deregulated environments [8].

Numerous efforts have been made to mitigate three-phase imbalance in DNSs, which can be roughly classified into three categories: feeder reconfiguration, phase swapping, and power regulation.

Feeder reconfiguration usually uses the controllable switches (automated/manual) throughout the network to change the topology of the system and thereby reduce the three-phase imbalance in the network. Ref. [9] presented a dynamic feeder reconfiguration method to mitigate voltage imbalance by mixed integer-linear programming (MILP) considering with DG outputs in DNSs. Ref. [10] presented a hierarchical decentralized feeder reconfiguration method for DNSs with DG connected, in which heuristic and genetic algorithm are combined to solve the reconfiguration problem to minimize the energy loss costs and DG operating costs simultaneously. Ref. [11] proposed a mixed-integer conic programming (MICP) formulation for the reconfiguration problem to minimize the power loss in a distribution network, and the authors believe that MICP is a preferable choice for network reconfiguration. Ref. [12] proposed a reconfiguration method based on improved selective binary particle swarm optimization algorithm to reduce the energy losses in DNSs. Ref. [13] proposed a mixed differential evolution algorithm combined with the algebraic connectivity in graph theory to solve the reconfiguration model to improve the three-phase imbalance problem in DNSs. However, the proposed method is only suitable for radial networks having few nodes only. Since the reconfiguration methods are primarily designed for relocating three-phase balanced load among feeders or isolate the fault section in DNSs to reduce network losses and improve power quality, it can just partially solve the three-phase imbalance problem [14].

Phase swapping is a straightforward way to balance a feeder by changing the connection of loads or lateral branches among phases. Ref. [15] first proposed phase swapping method to reduce the current imbalance in DNSs, and formulated the phase swapping model as a MILP problem. Ref. [16] proposed a method for simultaneous optimization of re-phasing, reconfiguration, and DG placement in DNSs to reduce three-phase imbalance and power losses. Ref. [17] suggested an online automatic commutation device and obtained the optimal control strategies based on the vector-genetic optimization algorithm to realize phase swapping in DNSs. Ref. [18] combined rephasing strategy and DG size adjustment simultaneously to achieve phase balance and minimize the system cost, and θ-modified bat algorithm was applied to solve the fuzzy multi-objective phase balancing problem. Besides, some other popular intelligence algorithms are also applied to seek optimal phase balancing solutions for DNSs, such as the genetic algorithm [19], particle swarm algorithm [20] and shuffled frog leaping algorithm [5]. The validity and effectiveness of intelligence algorithms on solving phase swapping problems were compared in [21]. Although significant progress has been made on phase swapping methods, there are still many factors that limit their applications. First of all, in order to achieve satisfactory control results, a large number of commutation switches should be installed at the three-phase nodes, which will cause substantial installation costs. Besides, the reliability of commutation channels, the accuracy of collected electrical signals and the computational speed of the control terminals should also be considered when applying this kind of methods. In addition, most existing studies only consider the static control of the switches, while the real load demand and DG output may vary dramatically with time, and thus it will be more realistic to consider the dynamic characteristics of DNSs.

Power regulation is also a conventional method to mitigate three-phase imbalance in DNSs, according to different principles, it can be divided into active power regulation, reactive power regulation, and hybrid regulation. Active power regulation is mainly based on energy storage devices, which achieves three-phase load balance by controlling the charging and discharging states of energy devices on each phase. Refs. [22,23] used ESSs to balance three-phase loads and minimize the power losses in DNSs. However, this regulation method will lead to frequent charging and discharging of ESSs, thereby shortening the life of energy storage devices. Moreover, the cost of current energy storage device is relatively high, which also limits the promotion and application of the method.

Reactive power regulation mainly relies on capacitors, static var compensators (SVCs) and other equipment to regulate the three-phase unbalanced loads through reactive power compensation, and the detailed principle is deduced in Section 2. Refs. [24,25] utilized SVCs and capacitors to compensate reactive power respectively, and both of them can dynamically adjust three-phase unbalanced loads to reduce the power losses and improve power factor in DNSs. However, the adjustment range of SVCs in [24] is limited in one three-phase line, and the capacitor compensation in [25] is easily lead to overcompensation. Ref. [26] proposed a flexible compensation strategy, which compensates the reactive power in DNSs by controlling the single-phase inverter of DGs to adjust the current imbalance in DNSs. However, the performance improvement in this method is at the expense of reducing the production of active power.

Hybrid regulation usually uses active power source and power electronic devices to adjust three-phase unbalanced loads in DNSs. Ref. [27] utilized the back-to-back inverters act as soft open points (SOPs) to mitigate three-phase imbalance and reduce the network power losses by controlling the active power flow and reactive power compensation in DNSs. However, this method will change the topology of the network, and the control of SOP is complex and will result in high energy losses. Ref. [28] proposed a method of using three-phase PV inverters and EV chargers to transfer power from highly loaded to less loaded phases to adjust the three-phase imbalance in DNSs. However, whether the EV owners are willing to participate in the unbalanced load regulation is

uncertain, and the control strategy is also a big challenge due to the method needs to control EV chargers and PV inverters at the same time.

Generally speaking, power compensation methods have a good effect on three-phase unbalanced loads regulation. However, current compensation methods mainly focus on the control strategy of an individual device and rarely consider the coordination of devices from the perspective of the entire system. Therefore, the adjustment range of the three-phase unbalanced load is limited.

In order to achieve the best adjustment effect, a device consisting of Y-connected and Δ-connected SVCs is applied in this paper. The device was firstly proposed in Ref. [7] and was mainly used to improve the load bus power factor of a three-phase four-wire feeder. However, according to our deduction, the device can transfer active power between phases while compensating reactive power on feeders. Therefore, it is used to mitigate the three-phase imbalance in DNSs and we name it as three-phase load-regulating device (TPLRD). Should be noted, TPLRD is not limited to constitute by SVCs, but can also be consisted of other advanced reactive power compensation devices.

Moreover, a joint optimization model based on TPLRD is proposed from the perspective of the whole system, which aims to mitigate the three-phase imbalance and minimize the active power losses of the whole system rather than a single feeder or particular area. Considering the fact that an increasing number of DGs and ESSs are connected to the distribution networks, the output constraints of DGs and the charging and discharging constraints of ESSs are taken into account. Meanwhile, the current imbalance and voltage imbalance are simultaneously considered in the model, while most of the existing methods focus only on one of them. Besides, some linearization techniques are introduced to transform the complex non-linear and non-convex optimization model into a MILP model, which results in significant improvement in the computational efficiency, and the errors caused by linearization also be analyzed.

The remainder of this paper is organized as follows. In Section 2, the three-phase balance principle of TPLRD is deduced and compares it with other three-phase unbalanced load regulating devices in the market. In Section 3, a joint optimization model is presented. In Section 4, case studies are conducted on the modified IEEE 34 and IEEE 123 test systems, and the errors caused by linearization methods are analyzed. The conclusions and outlook for future research are given in Section 5.

3. Introduction of TPLRD

3.1. Principle of TPLRD

The structure of TPLRD is shown in Fig. 1, which consists of Y-connected and Δ-connected SVCs. In Fig. 1 node i is a three-phase node, where the device is installed; V_a, V_b, V_c are the nodal voltages of phase a, b, c, respectively; I_a^Δ, I_b^Δ, I_c^Δ denote the three-phase injection currents from node i into Δ-connected SVCs, respectively; S_{ab}^Δ, S_{bc}^Δ, S_{ca}^Δ are the complex power produced by the Δ-connected SVCs; and S_a^Y, S_b^Y, S_c^Y are

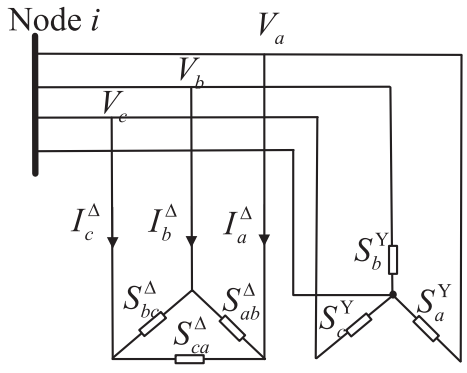

Fig. 1. The structure diagram of THLRD.

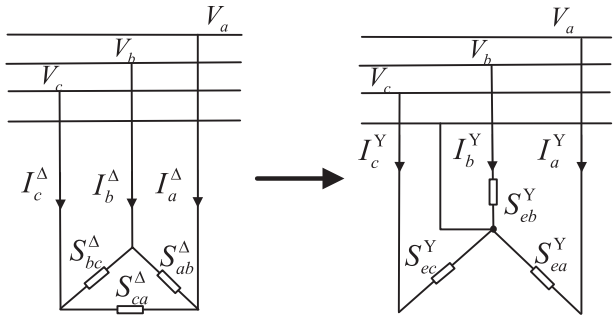

Fig. 2. Transformation diagram of Δ-connected SVCs.

the complex power produced by the Y-connected SVCs.

To simplify the analysis, the Δ-connected SVCs are transformed into the Y-connection, which is demonstrated in Fig. 2, where I_a^Y, I_b^Y, I_c^Y are the equivalent injection currents; S_{ea}, S_{eb}, S_{ec} are the equivalent complex power. Then, S_{ea} can be expressed as

$$S_{ea} = V_a I_a^Y = V_a\left(\frac{S_{ab}^\Delta}{V_{ab}} - \frac{S_{ca}^\Delta}{V_{ca}}\right). \tag{1}$$

If we assume the voltage of the same three-phase node is nearly balanced [29], the nodal voltage will satisfy

$$\frac{V_a}{V_b} \approx \frac{V_b}{V_c} \approx \frac{V_c}{V_a} \approx \varepsilon. \tag{2}$$

Therefore, Eq. (1) can be expressed as

$$S_{ea} \approx \frac{e^{-j\pi/6}}{\sqrt{3}} S_{ab}^\Delta - \frac{e^{-j5\pi/6}}{\sqrt{3}} S_{ca}^\Delta. \tag{3}$$

Similarly, S_{eb} and S_{ec} can be derived, and the equivalent power matrix of the Δ-connected SVCs is

$$\begin{pmatrix} S_{ea} \\ S_{eb} \\ S_{ec} \end{pmatrix} = \frac{1}{\sqrt{3}} \begin{pmatrix} e^{-j\pi/6} & 0 & -e^{-j5\pi/6} \\ -e^{-j5\pi/6} & e^{-j\pi/6} & 0 \\ 0 & -e^{-j5\pi/6} & e^{-j\pi/6} \end{pmatrix} \begin{pmatrix} S_{ab}^\Delta \\ S_{bc}^\Delta \\ S_{ca}^\Delta \end{pmatrix}. \tag{4}$$

Further, Eq. (4) can be expressed as

$$\begin{pmatrix} S_{ea} \\ S_{eb} \\ S_{ec} \end{pmatrix} = \frac{1}{\sqrt{3}} \begin{pmatrix} -\frac{\sqrt{3}}{2}(Q_{ab}^\Delta + Q_{ca}^\Delta)\,j + \frac{1}{2}(Q_{ca}^\Delta - Q_{ab}^\Delta) \\ -\frac{\sqrt{3}}{2}(Q_{ab}^\Delta + Q_{bc}^\Delta)\,j + \frac{1}{2}(Q_{ab}^\Delta - Q_{bc}^\Delta) \\ -\frac{\sqrt{3}}{2}(Q_{bc}^\Delta + Q_{ca}^\Delta)\,j + \frac{1}{2}(Q_{bc}^\Delta - Q_{ca}^\Delta) \end{pmatrix}, \tag{5}$$

where Q_{ab}^Δ, Q_{bc}^Δ, Q_{ca}^Δ are the reactive power produced by delta-connected SVCs. If write S_{ea}, S_{eb}, S_{ec} as

$$\begin{cases} S_{ea} = P_{ea} + jQ_{ea} \\ S_{eb} = P_{eb} + jQ_{eb}, \\ S_{ec} = P_{ec} + jQ_{ec} \end{cases} \tag{6}$$

where P_{ea}, P_{eb}, P_{ec}, Q_{ea}, Q_{eb}, Q_{ec} are the equivalent active and reactive power of phase a, b, c, respectively. Then, substituting Eq. (6) into Eq. (5), the equivalent active and reactive power produced by Δ-connected SVCs are

$$\begin{cases} P_{ea} = \frac{\sqrt{3}}{6}(Q_{ca}^\Delta - Q_{ab}^\Delta) \\ P_{eb} = \frac{\sqrt{3}}{6}(Q_{ab}^\Delta - Q_{bc}^\Delta) \\ P_{ec} = \frac{\sqrt{3}}{6}(Q_{bc}^\Delta - Q_{ca}^\Delta) \\ Q_{ea} = -\frac{1}{2}(Q_{ab}^\Delta + Q_{ca}^\Delta) \\ Q_{eb} = -\frac{1}{2}(Q_{ab}^\Delta + Q_{bc}^\Delta) \\ Q_{ec} = -\frac{1}{2}(Q_{bc}^\Delta + Q_{ca}^\Delta) \end{cases}. \tag{7}$$

Therefore, according to the superposition theorem, the equivalent

power produced by TPLRD can be expressed as

$$\begin{cases} \bar{P}_{ma,t} = \frac{\sqrt{3}}{6}(Q^{\Delta}_{ca,t} - Q^{\Delta}_{ab,t}) \\ \bar{P}_{mb,t} = \frac{\sqrt{3}}{6}(Q^{\Delta}_{ab,t} - Q^{\Delta}_{bc,t}) \\ \bar{P}_{mc,t} = \frac{\sqrt{3}}{6}(Q^{\Delta}_{bc,t} - Q^{\Delta}_{ca,t}) \\ \bar{Q}_{ma,t} = -\frac{1}{2}(Q^{\Delta}_{ab,t} + Q^{\Delta}_{ca,t}) + Q^{\mathrm{Y}}_{a,t} \\ \bar{Q}_{mb,t} = -\frac{1}{2}(Q^{\Delta}_{ab,t} + Q^{\Delta}_{bc,t}) + Q^{\mathrm{Y}}_{b,t} \\ \bar{Q}_{mc,t} = -\frac{1}{2}(Q^{\Delta}_{bc,t} + Q^{\Delta}_{ca,t}) + Q^{\mathrm{Y}}_{c,t} \end{cases}, \tag{8}$$

where the subscript 't' denotes the period t; 'm' is the node number; $Q^{\mathrm{Y}}_{a,t}$, $Q^{\mathrm{Y}}_{b,t}$, $Q^{\mathrm{Y}}_{c,t}$ are the reactive power produced by Y-connected SVCs; $\bar{P}_{ma,t}$, $\bar{P}_{mb,t}$, $\bar{P}_{mc,t}$, $\bar{Q}_{ma,t}$, $\bar{Q}_{mb,t}$, $\bar{Q}_{mc,t}$ are the equivalent active and reactive power produced by TPLRD. It can be observed from the first three equations of Eq. (8) that the sum of $\bar{P}_{ma,t}$, $\bar{P}_{mb,t}$, $\bar{P}_{mc,t}$ is zero, that is to say, the device could equivalently transfer active power among different phases by controlling Δ-connected SVCs. However, the active power equivalently transfer by Δ-connected SVCs may deteriorate the reactive power balance. Therefore, according to controlling Y-connected SVCs to compensate reactive power, which can not only eliminate adverse effects and balance reactive power, but also improve the load power factor.

3.2. Comparison with other regulating devices

As far as we know, there are mainly three kinds of three-phase unbalanced load regulating devices in the market, and some of them have been tried in DNSs on a small scale. They are the re-phasing switch based devices, the capacitor compensation based devices, and the power electronics based devices, respectively. The re-phasing switch based devices adjust three-phase unbalanced loads by changing the phase connection of loads or lateral branches among phases. The capacitor compensation based devices equivalently transfer active power between different phases through Δ-connected capacitors. The power electronics based devices regulate three-phase imbalance by controlling the turn-on and turn-off of high-power power electronics (e.g. GTO, GTR, and IGBT). Their advantages and disadvantages with TPLRD are shown in Table 1.

It can be seen From Table 1 that TPLRD has some advantages in common with the capacitor compensation based devices. However, since TPLRD is composed of Y-connected and Δ-connected SVCs, it has the advantages of fast response, continuous adjustment, and no over-compensation risk compared with capacitor compensation based devices. Although the investment cost of TPLRD is slightly higher than that of capacitor compensation based devices, the design life of current SVC is 20 years, and uses no inrush contactor or thyristor contactless switch which supports frequent switching, therefore, the cost-effectiveness of TPLRD is higher in the long run. In addition, compared to re-phasing based and power electronics based devices, TPLRD has the advantages of low power losses, low investment cost, and can improve power factor and voltage waveform by reactive power compensation. Besides, by adopting appropriate control strategies, harmonics can be suppressed and resonance can be avoided [30]. Therefore, TPLRD has better performance than the existing three-phase unbalanced load regulating devices, and if some reasonable global optimizations are achieved, the device can play an important role in DNSs.

4. Problem formulation

In order to mitigate the three-phase imbalance and minimize the active power losses, a joint optimization model based on TPLRD is established from the perspective of the whole system, and the decision variable of the model is the reactive power compensation amount of all TPLRDs. Besides, some constraints are also considered in this section.

4.1. Objective function

The most commonly used objective function in a DNS model is to minimize total active power losses or to minimize total operating costs. In this paper, the objective of the model is to minimize the total active power losses, and the objective function is shown in Eq. (9), where ∅ indicates the element-wise division. Besides,

$$\min \sum_{t\in \mathrm{T}} \sum_{(i,j)\in B} \boldsymbol{r}_{ij}[(\boldsymbol{P}_{ij,t})^2 + (\boldsymbol{Q}_{ij,t})^2] \varnothing (\boldsymbol{V}_{i,t})^2. \tag{9}$$

4.2. Constraints

4.2.1. Power flow constraint

For each node, the active power and reactive power must be balanced. In this paper, a linear power flow (LPF) model for DNSs [9] is used:

$$\sum_{k:(k,i)\in B} \boldsymbol{P}_{ki,t} + \sum_{f:f=i,f\in F} \boldsymbol{P}_{f,t} + \sum_{g:g=i,g\in G} \boldsymbol{P}_{g,t} + \sum_{e:e=i,e\in E} \boldsymbol{P}_{e,t} = \sum_{j:(i,j)\in B} \boldsymbol{P}_{ij,t} + \sum_{l:l=i,l\in L} \boldsymbol{P}_{l,t} + \sum_{m:m=i,m\in M} \bar{\boldsymbol{P}}_{m,t}, \tag{9a}$$

$$\sum_{k:(k,i)\in B} \boldsymbol{Q}_{ki,t} + \sum_{f:f=i,f\in F} \boldsymbol{Q}_{f,t} + \sum_{g:g=i,g\in G} \boldsymbol{Q}_{g,t} + \sum_{e:e=i,e\in E} \boldsymbol{Q}_{e,t} = \sum_{j:(i,j)\in B} \boldsymbol{Q}_{ij,t} + \sum_{l:l=i,l\in L} \boldsymbol{Q}_{l,t} + \sum_{m:m=i,m\in M} \bar{\boldsymbol{Q}}_{m,t}, \tag{9b}$$

$$\begin{cases} \boldsymbol{U}_{j,t} = \boldsymbol{U}_{i,t} - \tilde{\boldsymbol{Z}}_{ij}\boldsymbol{S}^{*}_{ij,t} - \tilde{\boldsymbol{Z}}^{*}_{ij}\boldsymbol{S}_{ij,t} \\ \tilde{\boldsymbol{Z}}_{ij} = \boldsymbol{\gamma} \odot \boldsymbol{Z}_{ij} \end{cases}, \tag{9c}$$

Table 1
The advantages and disadvantages of different devices.

Types	Advantage	Disadvantage
Re-phasing switch based	1. Low power loss 2. Three-phase imbalance can be practically solved on the load side	1. Influencing power supply reliability 2. Large demand and high cost
Capacitor compensation based	1. Low cost and low power loss 2. Easy to install 3. Can compensate reactive power and improve voltage waveform	1. Compensation accuracy is poor and can't be adjusted continuously 2. Easy lead to over-compensation 3. Slow response
Power electronics based	1. High compensation accuracy 2. Response quickly 3. Easy to install 4. Can compensate reactive power and filter simultaneously	1. High power loss and high cost 2. Control complexity
TPLRD	1. Low power loss and low cost 2. Easy to install 3. Continuous adjustment and high compensation accuracy 4. Can compensate reactive power and improve voltage waveform	1. May generate harmonics and resonance

$$\gamma = \begin{bmatrix} 1 & \varepsilon & \varepsilon^2 \\ \varepsilon^2 & 1 & \varepsilon \\ \varepsilon & \varepsilon^2 & 1 \end{bmatrix}, \tag{9d}$$

where $\boldsymbol{U}_{i,t} = [|V_{i,t}^a|^2 \ |V_{i,t}^b|^2 \ |V_{i,t}^c|^2]^{\mathrm{T}}$, $\boldsymbol{U}_{j,t} = [|V_{j,t}^a|^2 \ |V_{j,t}^b|^2 \ |V_{j,t}^c|^2]^{\mathrm{T}}$; $\boldsymbol{Z}_{ij}$ is the complex impedance matrix of branch ij; γ is a constant matrix; symbol $\odot$ denotes the element-wise product, and superscript * denotes the complex conjugate. Constraints (9a) and (9b) denote the active and reactive power are balanced at node i, respectively, and constraint (9c) is a linearized node voltage equation [9].

4.2.2. The constraints of DG output

$$\boldsymbol{P}_g^{\min} \leqslant \boldsymbol{P}_{g,t} \leqslant \boldsymbol{P}_g^{\max} \quad , \quad g \in G \quad , t \in T, \tag{10a}$$

$$\frac{\boldsymbol{P}_{g,t}}{\sqrt{(\boldsymbol{P}_{g,t})^2 + (\boldsymbol{Q}_{g,t})^2}} \geqslant \lambda_g^{\min} \quad , \quad g \in G, \quad t \in T, \tag{10b}$$

$$(\boldsymbol{P}_{g,t})^2 + (\boldsymbol{Q}_{g,t})^2 \leqslant (\boldsymbol{S}_g^{\max})^2 \quad , \quad g \in G \quad , t \in T, \tag{10c}$$

where $\boldsymbol{P}_g^{\min}$, $\boldsymbol{P}_g^{\max}$ are the lower and upper limits of DG output power; $\boldsymbol{S}_g^{\max}$ is the rated capacity of DG; $\lambda_g^{\min}$ is the minimum power factor of DG. Constraint (10b) indicates the output power of DG must meet the minimum power factor requirement, and constraint (10c) is the capacity limit of DG.

4.2.3. The constraint of branch capacity

$$(\boldsymbol{P}_{ij,t})^2 + (\boldsymbol{Q}_{ij,t})^2 \leqslant (\boldsymbol{S}_{ij}^{\max})^2 \quad , \quad (i, j) \in B, t \in T, \tag{11}$$

where $\boldsymbol{S}_{ij}^{\max}$ is the rated capacity of the branch ij, and constraint (11) guarantees that the branch power flow is within the limitations.

4.2.4. The constraint of voltage magnitude

$$U_{f,t} = |\boldsymbol{V}_f^{\mathrm{ref}}| \quad ^2 \ , \quad f \in F, t \in T, \tag{12a}$$

$$|\boldsymbol{V}_i^{\min}|^2 \leqslant U_{i,t}^2 \leqslant |\boldsymbol{V}_i^{\max}|^2 \quad , \quad i \in B, t \in T, \tag{12b}$$

where $\boldsymbol{V}_f^{\mathrm{ref}}$ is the voltage reference of the root node, and its default value is 1.0 pu; $U_{i,t}^2$ is the squared voltage magnitude of node i; $\boldsymbol{V}_i^{\min}$ and $\boldsymbol{V}_i^{\max}$ are the lower and upper limits of voltage magnitude at node i. Constraint (12b) denotes the squared voltage magnitude constraint.

4.2.5. The constraint of voltage imbalance

In practice, voltage imbalance is a major concern for unbalanced DNS. There are different definitions of voltage imbalance degree. In this paper, the maximum squared difference of the three-phase voltage magnitude divided by the mean of squared voltage magnitude is used (13a). According to American national standard ANSI C84.1-2011 [31], the voltage imbalance should be within 3%, which corresponds to a squared voltage imbalance of approximately 6% [32]. Therefore, the constraint for voltage imbalance is

$$VUF_{i,t} = \left| \frac{U_{i,t}^{\phi} - U_{i,t}^{ave}}{U_{i,t}^{ave}} \right| \leqslant 6\% \quad , \quad \phi = \{a, b, c\}, i \in N, t \in T, \tag{13a}$$

$$U_{i,t}^{ave} = \frac{1}{3} \sum_{\phi \in \Phi} U_{i,t}^{\phi} \quad , \quad i \in N, t \in T, \tag{13b}$$

where ϕ is the set of phase a, b, c; and $U_{i,t}^{\phi}$ denotes the square of the voltage of different phases.

4.2.6. The constraints of ESS

ESSs can play an important role in distribution network, such as energy arbitrage, peak shaving, ancillary support, voltage support, etc. Meanwhile, it can also be used for three-phase imbalance regulation, and the main principle is that in the heavy-loaded lines, the energy storage devices act as power sources to supply power to the loads by discharging, thereby reducing the power flowing from the distribution transformer to the heavy-loaded lines. On the contrary, in the light-loaded lines, the energy storage devices act as loads to increase the power demand by charging, thereby increasing the power flowing from the distribution transformer to the light-loaded lines. The constraints of ESS are as follows

$$0 \leqslant P_{e,t}^{\mathrm{c}} \leqslant \rho_{e,t}^{\mathrm{c}} P_{e,t}^{\max} \quad , \quad e \in E, t \in T, \tag{14a}$$

$$0 \leqslant P_{e,t}^{\mathrm{d}} \leqslant \rho_{e,t}^{\mathrm{d}} P_{e,t}^{\max} \quad , \quad e \in E, t \in T, \tag{14b}$$

$$\rho_{e,t}^{\mathrm{c}} + \rho_{e,t}^{\mathrm{d}} \leqslant 1 \quad , \quad e \in E, t \in T, \tag{14c}$$

$$SOC_{e,t} = SOC_{e,t-1} + \eta^{\mathrm{c}} P_{e,t}^{\mathrm{c}} - P_{e,t}^{\mathrm{d}}/\eta^{\mathrm{d}} \quad , \quad e \in E, t \in T, \tag{14d}$$

$$SOC_e^{\min} \leqslant SOC_{e,t} \leqslant SOC_e^{\max} \quad , \quad e \in E, t \in T, \tag{14e}$$

$$(P_{e,t}^{\mathrm{c}})^2 + (Q_{e,t}^{\mathrm{c}})^2 \leqslant (S_e^{\max})^2, \quad e \in E, t \in T, \tag{14f}$$

$$(P_{e,t}^{d})^2 + (Q_{e,t}^{\mathrm{d}})^2 \leqslant (S_e^{\max})^2 \quad , \quad e \in E, t \in T, \tag{14g}$$

where $SOC_e^{\max}$ and $SOC_e^{\min}$ are the upper and lower limits of SOC; $P_{e,t}^{\max}$ is the maximum active output of the inverter; $S_e^{\max}$ is the maximum capacity of the inverter connected with ESS. Constraints (14a) and (14b) are the charging and discharging power restrictions; constraint (14c) denotes the operation constraint of ESS; constraint (14d) indicates the impact of charging and discharging on SOC, and constraint (14e) reflects the lower and upper bounds of SOC; constraints (14f) and (14g) indicate the capacity restriction of ESS.

4.2.7. The constraints of TPLRD

Eq. (8) shows the relationship between the equivalent active and reactive power produced by TPLRD. Let

$$\begin{cases} Q_{\min}^{\Delta} \leqslant Q_{ab,t}^{\Delta}, & Q_{bc,t}^{\Delta}, & Q_{ca,t}^{\Delta} \leqslant Q_{\max}^{\Delta} \\ Q_{\min}^{\mathrm{Y}} \leqslant Q_{a,t}^{\mathrm{Y}}, & Q_{b,t}^{\mathrm{Y}}, & Q_{c,t}^{\mathrm{Y}} \leqslant Q_{\max}^{\mathrm{Y}} \end{cases}, \tag{15}$$

then the reactive power compensation status of TPLRD can be known at each time, and constraint (15) indicates the compensation capacity of each SVC is limited, therefore, in order to achieve the desired result, multiple TPLRDs are needed in DNSs.

In order to guarantee that the transformer operates within a certain power factor, constraint (16) is proposed, where P_a, P_b, P_c, Q_a, Q_b, Q_c are the primary active and reactive power demands of each phase in DNSs; P_a', P_b', P_c', Q_a', Q_b', Q_c' are the active and reactive power demands of each phase after regulating by THLRDs; θ is the power factor angle.

$$\begin{aligned} &Q_a' + Q' + \ Q_c' \leqslant (P_a' + P_b' + P_c')\arctan\theta \\ &\begin{cases} Q_a' = Q_a + \bar{Q}_{ma,t}, \quad Q_b' = Q_b + \bar{Q}_{mb,t}, \\ \quad Q_c' = Q_c + \bar{Q}_{mc,t} \\ P_a' = P_a + \bar{P}_{ma,t} \quad , \quad P_b' = P_b + \bar{P}_{mb,t} \quad , \\ P_c' = P_c + \bar{P}_{mc,t} \end{cases} \end{aligned} \tag{16}$$

4.2.8. The constraint of current imbalance

The current imbalance degree at the root node is an important indicator in DNSs, and it is defined as the absolute value of the positive sequence current divided by negative sequence current (17)

$$\begin{aligned} &CUF_{f,t} = \frac{|I_{f,t}^{+}|}{|I_{f,t}^{-}|} \leqslant CUF_f^{\max}, \quad f \in F, t \in T \\ &I_{f,t}^{-} = (I_{f,t}^{\mathrm{a}} + \varepsilon^2 I_{f,t}^{\mathrm{b}} + \varepsilon I_{f,t}^{\mathrm{c}})/3, \quad f \in F, t \in T \\ &I_{f,t}^{+} = (I_{f,t}^{\mathrm{a}} + \varepsilon I_{f,t}^{\mathrm{b}} + \varepsilon^2 I_{f,t}^{\mathrm{c}})/3, \quad f \in F, t \in T \end{aligned} \tag{17}$$

where $CUF_f^{\max}$ is the maximum current imbalance degree of root node.

Since constraints (10), (11), and (14) are non-linear quadratic

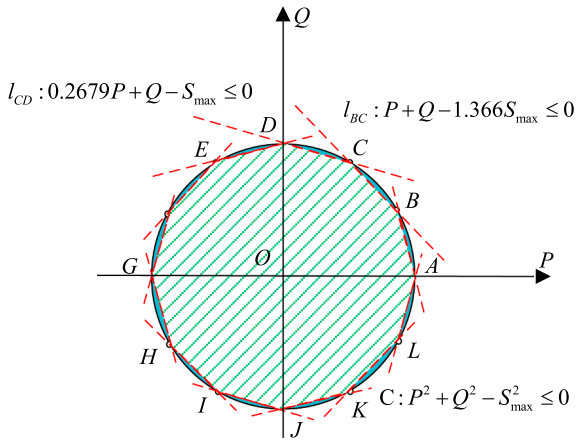

Fig. 3. Diagram of a polygonal inner-approximation method.

inequality constraints, and constraint (17) is a non-convex constraint. Hence the model is complex and challenging to solve. In the next section, the corresponding linearization techniques are introduced.

5. Linearization methods

5.1. Linearization of circular constraint

For quadratic non-linear inequality constraints (10), (11), and (14), a viable method is to convert them into regular polygon constraints. Ref. [33] used a regular polygon with 12 edges to linearize the quadratic inequality constraints and yielded a good result. In this paper, the same method is applied, and the principle demonstrated in Fig. 3. The feasible region limited by above quadratic inequalities is the interior area of the circle, whose radius is equal to $S^2_{\max}$.

The circular constraint will be satisfied only if the polygonal constraints are satisfied. Since the vertices of the regular polygon with 12 edges are located at the circumference and can be obtained easily. Therefore, it can be used to approximately transform the quadratic inequalities into a set of 12 linear inequality constraints. Taking lines l_{BC}, l_{CD} in Fig. 3 as the example, and the form of the constraint set shown as:

$$\alpha_k P+\beta_k Q+\chi_k S_{\max}\le 0,\quad k=\{1,2,3...12\}, \tag{18}$$

where P, Q, $S_{\max}$ denote the active, reactive and apparent power, respectively;α_k,β_k, χ_k are the coefficients of the k^{th} edge, and their values are listed in Table 2.

5.2. Linearization of non-convex constraint

According to the complex power equation $S=VI^*$, it can be modified to $I=(S/V)^*$. Therefore, $I^+_{f,t}$ can be rewritten as:

$$I^+_{f,t}=\frac{1}{3}\left(\left(\frac{S^a_{f,t}}{V^a_{f,t}}\right)^*+\varepsilon\left(\frac{S^b_{f,t}}{V^b_{f,t}}\right)^*+\varepsilon^2\left(\frac{S^c_{f,t}}{V^c_{f,t}}\right)^*\right). \tag{19}$$

where $S^a_{f,t}$, $S^b_{f,t}$, $S^c_{f,t}$ and $V^a_{f,t}$, $V^b_{f,t}$, $V^c_{f,t}$ are the apparent power and voltage of phase a, b, c, respectively. If we represent $V^b_{f,t}$ and $V^c_{f,t}$ by $V^a_{f,t}$, then Eq. (19) can be simplified as

$$I^+_{f,t}=\frac{1}{3}\left(\frac{(S^a_{f,t})^*}{(V^a_{f,t})^*}+\varepsilon\frac{(S^b_{f,t})^*}{(\varepsilon^{-1}V^a_{f,t})^*}+\varepsilon^2\frac{(S^c_{f,t})^*}{(\varepsilon V^a_{f,t})^*}\right)=\frac{1}{3(V^a_{f,t})^*}((S^a_{f,t})^*+(S^b_{f,t})^*+(S^c_{f,t})^*). \tag{20}$$

Similarly, $I^-_{f,t}$ can be derived

$$I^-_{f,t}=\frac{1}{3(V^a_{f,t})^*}((S^a_{f,t})^*+\varepsilon(S^b_{f,t})^*+\varepsilon^2(S^c_{f,t})^*). \tag{21}$$

Then the current imbalance degree can be transformed into

$$CUF_{f,t}=\left|\frac{S^a_{f,t}+\varepsilon^2S^b_{f,t}+\varepsilon S^c_{f,t}}{S^a_{f,t}+S^b_{f,t}+S^c_{f,t}}\right|\leqslant CUF^{\max}_f, \tag{22}$$

where $CUF^{\max}_f$ is the maximum current imbalance degree. A conservative linear approximation method proposed in Ref. [34] is used to transform the constraint (22) into a convex constraint set (23), and the detailed derivation is shown in Appendix A. Among the constraint set (23), δ defines how far the output power of the transformer at each phase can deviate from the average value of three-phase output power, and $CUF^{\max}_f$ is determined by δ. Table 3 lists the different value of δ corresponding to $CUF^{\max}_f$.

$$\begin{cases}(1-\delta)\frac{P^a_{f,t}+P^b_{f,t}+P^c_{f,t}}{3}\leqslant P^a_{f,t}\leqslant(1+\delta)\frac{P^a_{f,t}+P^b_{f,t}+P^c_{f,t}}{3}\\(1-\delta)\frac{P^a_{f,t}+P^b_{f,t}+P^c_{f,t}}{3}\leqslant P^b_{f,t}\leqslant(1+\delta)\frac{P^a_{f,t}+P^b_{f,t}+P^c_{f,t}}{3}\\(1-\delta)\frac{P^a_{f,t}+P^b_{f,t}+P^c_{f,t}}{3}\leqslant P^c_{f,t}\leqslant(1+\delta)\frac{P^a_{f,t}+P^b_{f,t}+P^c_{f,t}}{3}\end{cases},$$
$$\begin{cases}(1-\delta)\frac{Q^a_{f,t}+Q^b_{f,t}+Q^c_{f,t}}{3}\leqslant Q^a_{f,t}\leqslant(1+\delta)\frac{Q^a_{f,t}+Q^b_{f,t}+Q^c_{f,t}}{3}\\(1-\delta)\frac{Q^a_{f,t}+Q^b_{f,t}+Q^c_{f,t}}{3}\leqslant Q^b_{f,t}\leqslant(1+\delta)\frac{Q^a_{f,t}+Q^b_{f,t}+Q^c_{f,t}}{3}\\(1-\delta)\frac{Q^a_{f,t}+Q^b_{f,t}+Q^c_{f,t}}{3}\leqslant Q^c_{f,t}\leqslant(1+\delta)\frac{Q^a_{f,t}+Q^b_{f,t}+Q^c_{f,t}}{3}\end{cases} \tag{23}$$

According to the aforementioned process, the model can be transformed into a MILP model and solved by off-the-shelf commercial software. In this paper, CPLEX is utilized.

6. Case studies

The case studies are based on modified IEEE 34 and IEEE 123 test systems. Because the distribution network studied in this paper contains DGs and ESSs, and ESSs can also adjust three-phase imbalance [21,22], in order to verify the effectiveness of the proposed methods, four different comparison schemes are designed through different parameter settings in each case:

scheme 1 (Sch.1): without TPLRDs and ESSs in the DNS.
scheme 2 (Sch.2): with ESSs but no TPLRDs in the DNS.
scheme 3 (Sch.3): with TPLRDs but no ESSs in the DNS.
scheme 4 (Sch.4): with ESSs and TPLRDs in the DNS.

In addition, since linearization methods are used to convert the non-convex nonlinear model to a MILP model. In order to verify whether the errors from MILP model are acceptable, the optimization results of the non-linear programming (NLP) model and MILP model are compared based on Sch.4. Fig. 4 shows the flowchart of model solving (a) and the case study (b), where n is the number of iterations in the process of

Table 2
Coefficients of the linearized quadratic inequality constraints.

k	1	2	3	4	5	6	7	8	9	10	11	12
α_k	1	1	0.2679	−0.2679	−1	−1	−1	−1	−0.2679	0.2679	1	1
β_k	0.2679	1	1	1	1	0.2679	−0.2679	−1	−1	−1	−1	−0.2679
χ_k	−1	−1.366	−1	−1	−1.366	−1	−1	−1.366	−1	−1	−1.366	−1

Table 3
Different value of δ corresponding to $CUF_f^{\max}$.

δ	0.04641	0.09282	0.13923	0.18564	0.23205	0.27846	0.32487	0.37128
$CUF_f^{\max}$	0.05	0.1	0.15	0.2	0.25	0.3	0.35	0.4

solving, and $N_{\max}$ is the maximum number of iterations. Meanwhile, in order to quantify the imbalance of the three-phase loads, we defined the three-phase active/reactive power imbalance rate of the distribution transformer as

$$LF_{f,t} = \max\left(\frac{X_{f,t}^{\max} - X_{f,t}^{\min}}{X_{f,t}^{\max}}\right), \quad X = \{P, Q\}, i \in N, t \in T, \tag{24}$$

where X represents the active and reactive power flowing through the distribution transformer.

In addition, because binary variables $\rho_{e,t}^{c}$ and $\rho_{e,t}^{d}$ are used in the model to represent the charging and discharging state of ESSs, In order make the model suitable for non-linear programming solution, the binary variables $\rho_{e,t}^{c}$ and $\rho_{e,t}^{d}$ can be converted into continuous variable by using the method in [35], and the detail of the conversion is shown in Appendix B.

The daily variation coefficient of load is the same as that of Ref. [5] and the daily operation curves of DGs (PV and WG) are shown in Fig. 5. The lower and upper limits of voltage in DNSs are set to 0.95 and 1.05, respectively; the maximum voltage imbalance degree of the three-phase nodes is set to 3% [31]. The maximum current imbalance degree of the root node is set to 20% [36]. The lower and upper limits of *SOC* are set 0.2 and 0.9, respectively, and the initial value of *SOC* is set to 0.5. The power factor of the distribution transformer is set to 0.98. The compensation capacity of each SVC ranges from −100 kVar to 100 kVar. Moreover, both cases are solved by CPLEX 12.7 based on GAMS25.1.1 [37] on a personal computer with an Intel Core i5-3470 3.20GHZ CPU and 8 GB of RAM.

6.1. IEEE 34 test system

The modified IEEE 34 test system topology is shown in Fig. 6, the number one node is the root node, and it is connected to the secondary side of the transformer. The capacity of the transformer is 5000 kVA. The rated voltage level is 29.6 kV, the total active and reactive power loads in each phase is 1309.3 kW/795.2 kVar, 1623 kW/928.1 kVar, and 970 kW/589.8 kVar, respectively. Besides, in Fig. 6 the solid lines represent the three-phase feeders with three- or single-phase loads. The dash lines denote the single-phase feeders, which only connected with single-phase loads. In this case, there are five DGs and two ESSs considered, their capacities and locations are shown in Table 4. To examine the effect of TPLRD, five more TPLRDs are installed close to DGs, their locations are shown in Fig. 5.

Firstly, the hourly active and reactive power balance results of each phase are compared. Fig. 7 shows the hourly balance results under different schemes, and Table 5 lists the hourly three-phase load imbalance under different schemes. Should be noted that the active and reactive power we calculated is the total power flowing through the transformer. Therefore, when there are devices to compensate reactive power in DNSs, the total reactive power flowing through the transformer will reduce.

From Fig. 7, it can be clearly seen that the active/reactive power flowing through the transformer are unbalanced in Sch.1, and according to Table 5 it can be found that during peak load period the maximum active/reactive power imbalance as higher as 53% and 51.9%, respectively. Even the minimum active/reactive power imbalance degree is still 36.9% and 22.9%, respectively. When two ESSs are utilized in Sch.2, the active power imbalance is reduced, the maximum value in the same peak load period is 10.7%. However, the

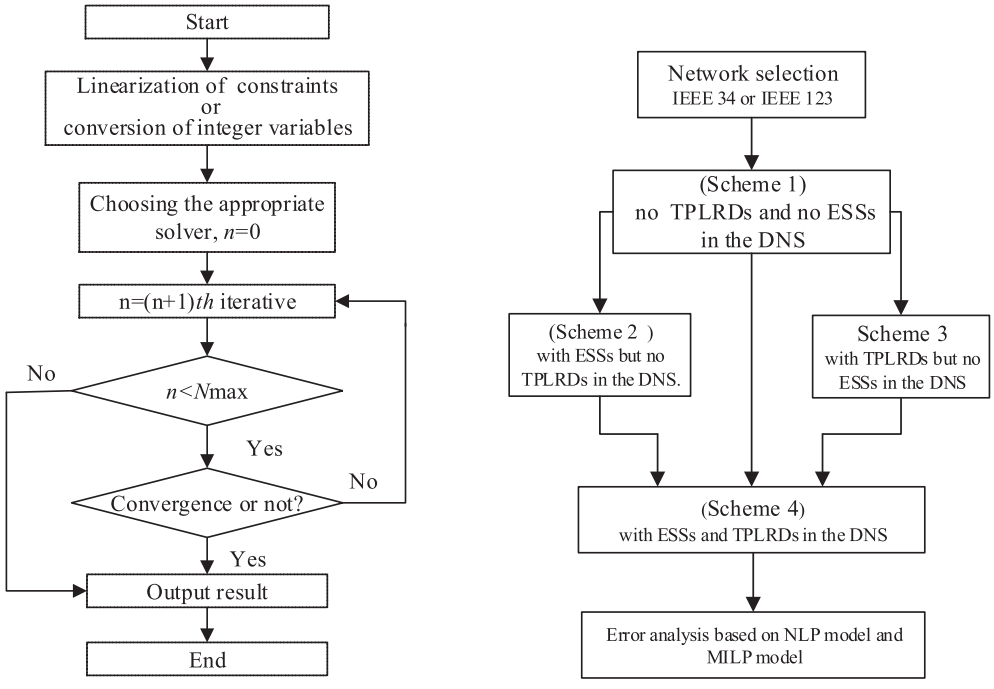

(a) The model solving flowchart (b) The case study flowchart

Fig. 4. The model solving flowchart and the case study flowchart.

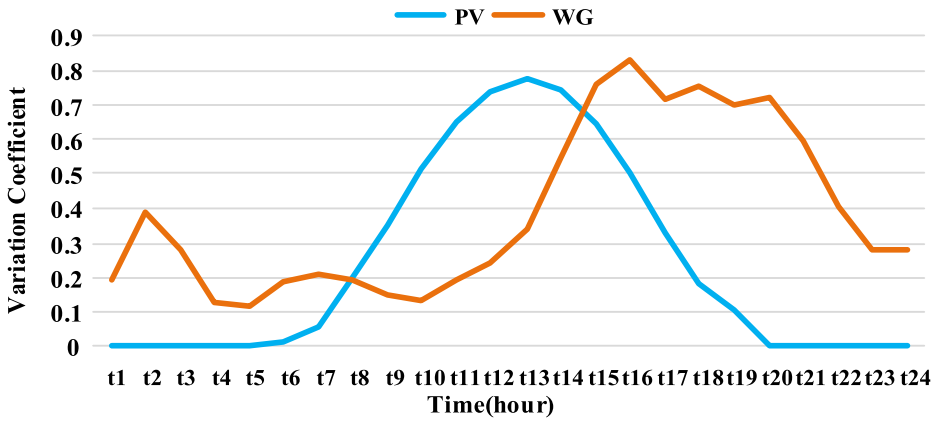

Fig. 5. Operation curves of PV and WG.

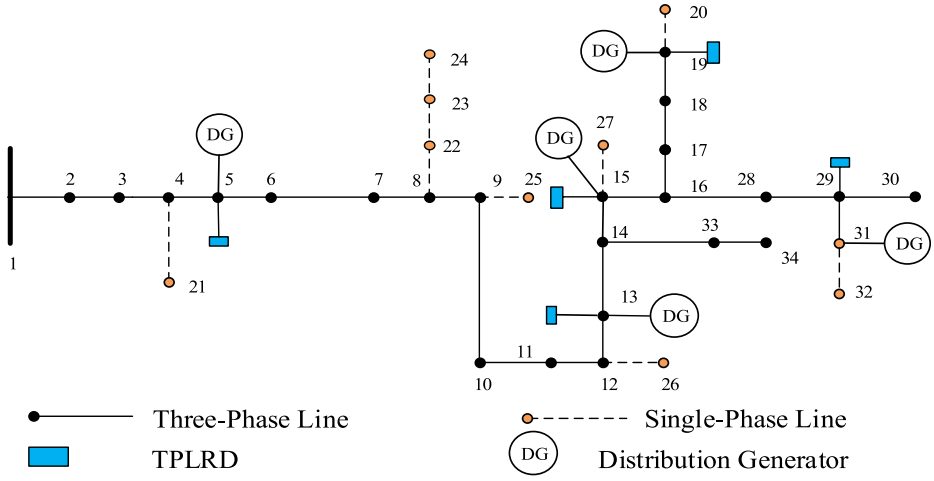

Fig. 6. Modified IEEE 34 test system.

Table 4
The location and capacity of DGs and ESSs.

	PV1 (kW)	PV2 (kW)	PV3 (kW)	WG1 (kW)	WG2 (kW)	ESS1 (kW)	ESS2 (kW)
Location	5	13	27	19	31	7	16
a	100	150	0	100	150	200	200
b	100	150	0	100	0	200	200
c	100	150	100	100	0	200	200

reactive power adjustment effect is not very good due to the reactive power compensation capability of ESS is limited. In Sch.3, only five TPLRDs are involved in unbalanced load regulation, it can be seen from Fig. 7 that TPLRDs can significantly reduce the three-phase active/reactive power imbalance, and the maximum active power imbalance is 5.6%, the reactive power is also approximately balanced. In Sch.4, two ESSs are added to the model on the basis of Sch.3. From Fig. 7 it can be found that the imbalance of three-phase active power is further reduced compared with that of in Sch.3, and the maximum active power imbalance is 2.92%, the reactive power imbalance degree still maintained at a low level according to the data in Table 5.

In addition, the active power losses, current imbalance degree of the root node and voltage imbalance degree of three-phase nodes are also compared under four different schemes. Figs. 8–10 illustrate the comparison results.

Fig. 8 shows the hourly active power losses, it can be seen that the active power losses under four schemes are reduced in turn. The total active power losses in Sch.1 is 2370.7 kWh. When ESSs are applied in Sch.2, the total active power losses reduced to 1926.34 kWh, and the reduction relative to Sch.1 is 18.7%. However, when TPLRDs are applied in Sch.3, the total active power losses reduced to 1601.37 kWh, and the reduction relative to Sch.1 is 32.45%. When ESSs and TPLRDs are both applied in Sch.4, the total active power losses are 1560.2 kWh and the reduction relative to Sch.1 is 34.2%. The result shows that our method has good energy saving effect.

Fig. 9 illustrates the hourly current imbalance degree curves, the maximum $CUF_{f,t}$ is 44.13% and exceeds the 20% limit in Sch.1. Although the current imbalance curve becomes relatively flat when the ESSs are applied in Sch.2, the $CUF_{f,t}$ still exceeds the limitation during peak load period. However, when TPLRDs are applied in Sch.3, the curve is very flat, the $CUF_{f,t}$ is maintained less than 5%, which is much better than that of in Sch.1 and Sch.2. In Sch.4, even though the ESSs and TPLRDs are both applied, the change is not significant compared to that of in Sch.3. The results show that our methods can effectively reduce the current imbalance in DNSs.

Fig. 10 shows the comparison of the maximum voltage imbalance degree. It can be noticed that as the distance between the root node and other nodes increases, the maximum voltage imbalance increases as well. And there are many nodes in Sch.1 that their maximum voltage imbalance exceeded 3%. However, when ESSs are applied in Sch.2, the maximum voltage imbalance of the three-phase nodes is significantly reduced, which means ESSs can adjust the voltage imbalance in DNSs. However, when TPLRDs are applied in Sch.3 and Sch.4, the voltage imbalance is further reduced compared to that of in Sch.2. The results show that our methods have an advantage in adjusting the voltage imbalance.

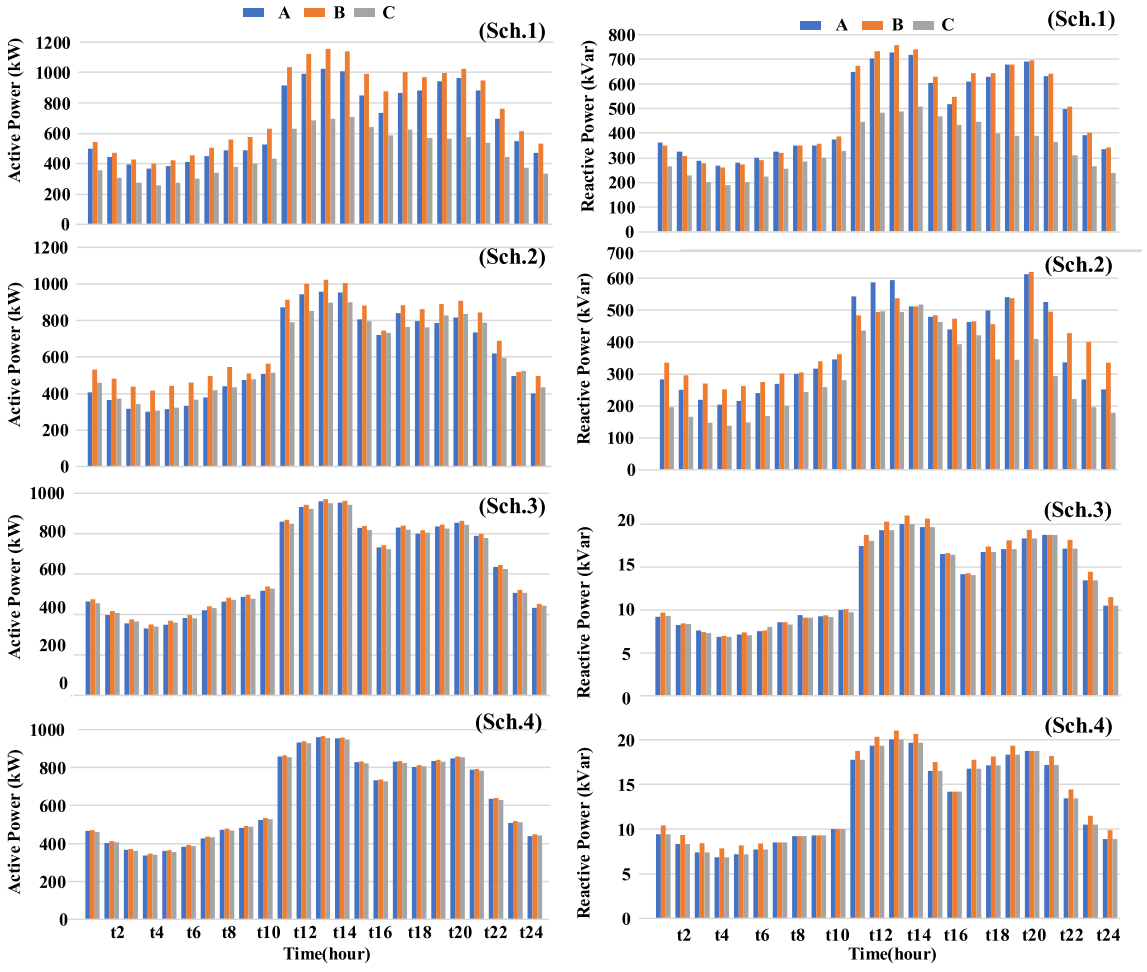

Fig. 7. Hourly comparison of active /reactive power flowing through the transformer.

According to the comparison of different schemes, it can be found that ESSs can adjust the three-phase imbalance of DNSs, but the regulating effect is not ideal, especially for the regulation of reactive loads and current imbalance. However, the methods proposed in this paper can achieve a better effect, it can not only mitigate the three-phase imbalance, reduce the active power losses, but also reduce the voltage and current imbalance at the same time.

In order to verify whether the calculation errors are acceptable due to the loss of some feasible regions during the linearization process, the active power losses based on the NLP model and the MILP model are compared, and the comparison results show in Table 6. According to the comparison of the hourly power losses of two models, the maximum error occurs at *t20*, and the calculated difference is 7.2 kWh, and the relative error is 4.79%. However, comparing the total power losses for 24 h, the optimization results based on MILP model and NLP model are 1560.2 kWh and 1533.6 kWh, respectively, and the relative error is only 1.79%. It can be seen that the errors caused by linearization are relatively small and within a acceptable range. Meanwhile, the total

Table 5
Hourly active/reactive power imbalance (%) comparison for different schemes.

Time	Active Power imbalance				Reactive power imbalance				Time	Active power imbalance				Reactive power imbalance			
	Sch.1	Sch.2	Sch.3	Sch.4.4	Sch.1	Sch.2	Sch.3	Sch.4		Sch.1	Sch.2	Sch.3	Sch.4	Sch.1	Sch.2	Sch.3	Sch.4
t1	40.9	27.3	4.21	2.11	29.5	51.2	2.31	10.2	t13	48.2	13.0	2.06	1.46	41.0	18.5	4.75	5.12
t2	41.2	28.9	4.79	2.46	33.4	45.9	6.78	11.5	t14	45.6	11.1	2.07	1.73	35.6	1.18	4.83	4.93
t3	42.6	33.2	5.32	2.71	33.3	58.0	4.45	12.9	t15	42.4	10.2	2.38	1.26	28.2	4.84	1.20	5.04
t4	41.8	33.9	5.60	2.92	33.3	57.8	4.48	12.9	t16	40.1	3.18	2.69	1.29	22.9	18.3	1.41	5.92
t5	41.8	35.7	5.41	2.75	30.9	54.5	7.71	13.3	t17	45.5	14.5	2.38	1.26	34.9	9.64	3.61	1.07
t6	39.8	32.8	4.40	2.25	27.8	46.6	2.52	8.33	t18	49.3	12.4	2.13	1.27	42.7	35.4	5.51	5.84
t7	38.8	27.4	4.53	2.37	23.4	39.3	5.79	7.31	t19	51.9	12.3	2.36	1.12	49.7	41.5	5.16	5.74
t8	38.1	23.6	4.14	2.13	19.9	31.7	1.63	1.07	t20	53.0	10.7	2.31	1.19	51.9	35.4	1.16	5.36
t9	36.9	17.6	4.02	2.15	16.7	26.4	1.74	2.36	t21	52.4	13.8	2.51	1.27	50.7	52.9	5.50	1.57
t10	37.0	10.4	3.71	1.86	16.5	24.6	2.45	7.23	t22	49.9	14.8	3.10	1.58	45.1	48.2	6.91	5.74
t11	47.1	14.3	2.31	1.27	38.6	21.9	5.34	5.52	t23	46.7	5.42	2.88	1.97	38.2	49.6	8.67	7.26
t12	47.3	15.9	2.12	1.19	39.1	17.5	4.92	5.10	t24	44.6	21.8	4.42	2.02	33.6	51.6	5.29	9.28

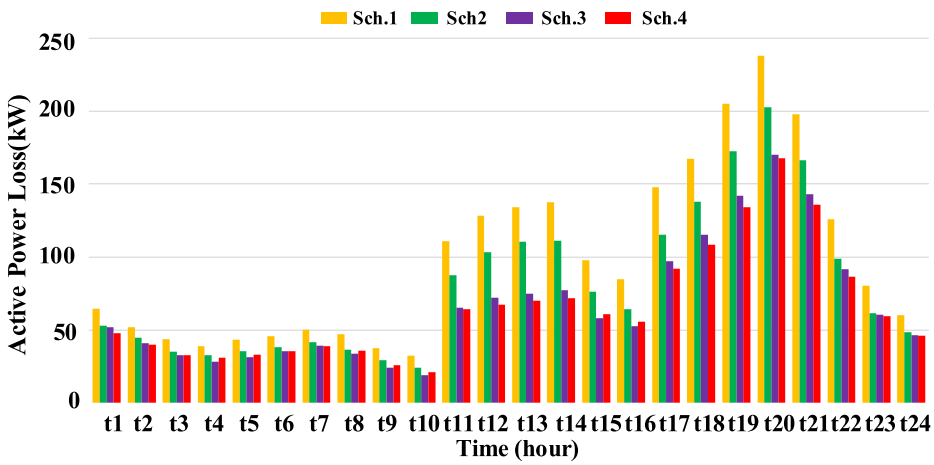

Fig. 8. The hourly comparison of active power losses.

execution time of the two models is also compared. The solution time of MILP model is 2.28 s and that of NLP model is 206.8 s. It can be seen that although MILP model sacrifices some calculation accuracy, it greatly improves the calculation efficiency.

6.2. IEEE 123 test system

In order to illustrate the scalability of the method, it is conducted on a modified IEEE 123 test system. Fig. 11 depicts the network topology of the system, the solid lines denote three-phase feeders, and the dash lines indicate the two- or single-phase feeders, the black, green and brown solid cycles signify three-, two- and single-phase nodes, respectively. In this case, 8 DGs and 2 ESSs are considered, and their capacities and locations are listed in Table 7. Moreover, eight more TPLRDs are installed at eight three-phase nodes close to DGs, and their locations are also shown in Fig. 11.

Firstly, the hourly active and reactive power balance results under different schemes are compared. Fig. 12 shows the hourly comparison of active/reactive power flowing through the transformer under different schemes. Table 8 lists the hourly power imbalance rate under different schemes. It can be found from Fig. 12 that the phase loads distribution is uneven in Sch.1, and the active and reactive power imbalance rates at time *t20* are 49.1% and 32.6%, respective. When ESSs are applied in Sch.2, the active and reactive power imbalance degrees are reduced, but during peak load period the active and reactive power imbalance are still large, the values at time *t20* are 17.2% and 30.1%, respectively. However, when eight TPLRDs are applied in Sch.3, the active and reactive power are balanced very well, and the active and reactive power imbalance at time *t20* are 3.14% and 4.46%, respectively. In Sch.4, both ESSs and TPLRDs are applied, it can be seen that the effect of three-phase load balancing in Sch.4 is slightly better than that in Sch.3, and the active and reactive load distributions are approximately balanced.

Figs. 13–15 illustrate the comparison of the active power losses, current imbalance degree of the root node and voltage imbalance degree of three-phase nodes for three different schemes. It can be seen from Fig. 13 that the total active power losses in Sch.1 is 202.7 kWh. When ESSs are applied in Sch.2, the total active power losses reduced to 170.9 kWh, the reduction is 15.68%. Compared with Sch.1, when TPLRDs are applied in Sch.3, the total active power losses reduced to 141.4 kWh, and the reduction is 30.2%. However, when TPLRDs and ESSs are both applied in Sch.4, the total active power losses reduced to 130.2 kWh and the reduction is 35.6%.

Fig. 14 shows the hourly current imbalance comparison. In Sch.1 the maximum $CUF_{f,t}$ is 40.7%, which exceeds 20%. When ESSs are applied in Sch.2, the curve dropped obviously, but there still exists a short period of time that $CUF_{f,t}$ exceeds 20%. In Sch.3, the maximum $CUF_{f,t}$ is 14.6%, which indicates that TPLRD has a good effect in reducing the current imbalance. Moreover, when TPLRDs and ESSs are both applied in Sch.4, the current imbalance curve is maintained at a level below 8%. Fig. 15 shows the maximum voltage imbalance degree comparison. It can be found that there are only a few nodes which far away from the root node exceed 3% in Sch.1. When ESSs or TPLRDs are applied in Sch.2 and Sch.3, respectively, the maximum voltage imbalance degree is reduced obviously, and the voltage imbalance in Sch.3 is reduced more. Further, when TPLRDs and ESSs are both applied in Sch.4, the voltage imbalance degree is further reduced, albeit not much. According to the comparison results of four different

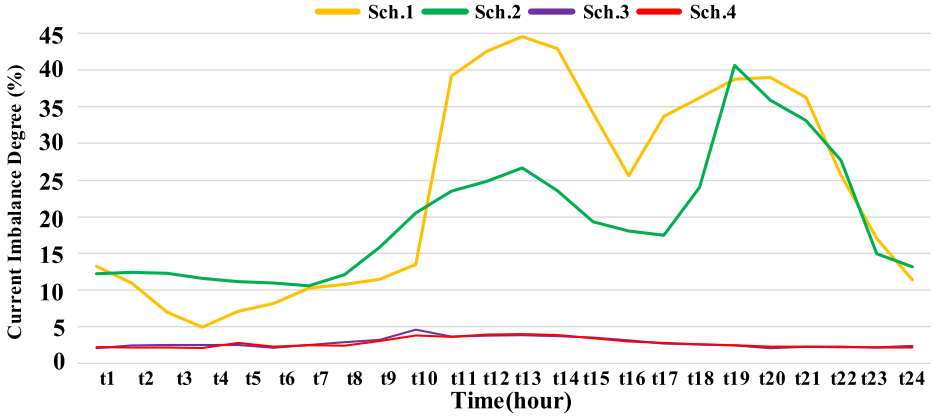

Fig. 9. The hourly comparison of root node current imbalance degree.

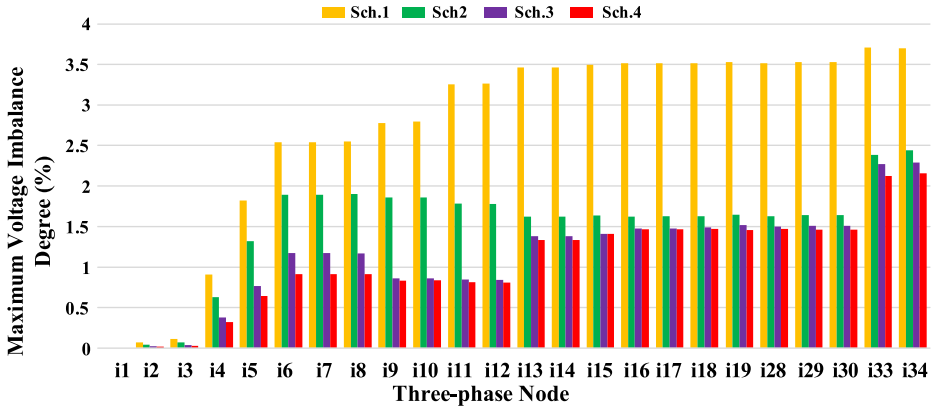

Fig. 10. The comparison of maximum voltage imbalance degree of three-phase nodes.

Table 6
The comparison of hourly active power losses (kWh) in IEEE 34 test system.

Time period	t1	t2	t3	t4	t5	t6	t7	t8	t9	t10	t11	t12
NLP	46.98	40.74	34.42	31.58	34.16	36.31	39.64	36.61	26.39	21.34	63.18	64.08
MILP	47.71	39.76	32.75	30.95	32.91	35.33	38.91	35.71	25.80	20.82	64.11	67.33
Hourly error	1.56%	2.41%	4.86%	2.00%	3.66%	2.68%	1.82%	2.44%	2.25%	2.41%	1.46%	3.91%
Time period	t13	t14	t15	t16	t17	t18	t19	t20	t21	t22	t23	t24
NLP	67.31	69.54	58.51	57.21	89.63	106.0	130.3	160.2	132.3	84.31	57.53	44.41
MILP	70.09	71.76	60.65	55.53	91.91	108.4	134.0	167.9	135.9	86.38	59.20	46.10
Hourly error	4.13%	3.18%	3.64%	2.93%	2.53%	2.29%	2.83%	4.79%	2.72%	2.45%	2.91%	3.80%
MODEL	NLP		MILP		Total error		Calculation time		NLP		MILP	
Power losses	1533.6 kWh		1560.2 kWh		1.79%				206.82 s		2.28 s	

schemes, it can be found that even in a large network our methods can still guarantee good results, and it also proves that our method has good scalability.

Table 9 gives the comparison of active power losses of two different models, it can be seen that although the optimization results of two models are different, the difference is not obvious. The maximum error still occurs at *t20*, the calculated difference is 0.687 kWh and the corresponding relative error is 4.83%. In addition, the total power losses

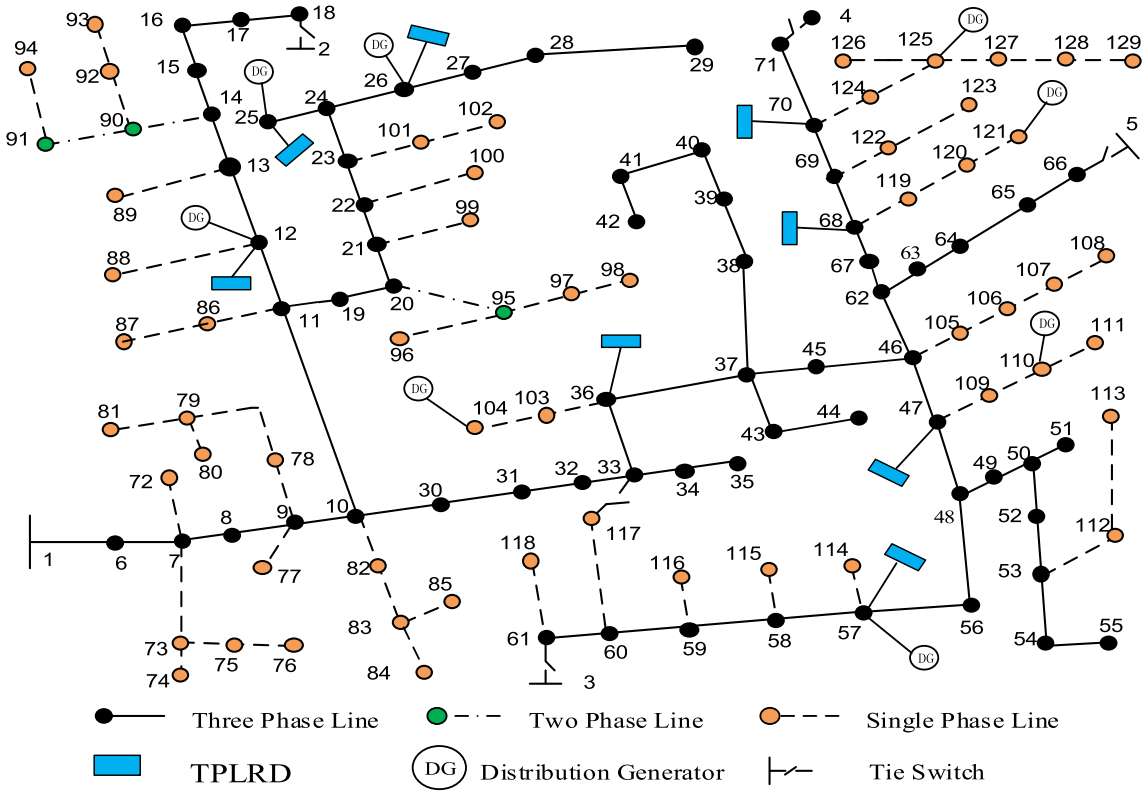

Fig. 11. Modified IEEE 123 test system.

Table 7
The Locations and capacities of DGs and ESSs.

	NODE	Phase-a	Phase-b	Phase-c		Node	Phase-a	Phase-b	Phase-c
PV1 (kW)	12	50	50	50	WG1 (kW)	57	50	50	50
PV2 (kW)	25	50	50	50	WG2 (kW)	121	0	100	0
PV3 (kW)	26	50	50	50	WG3 (kW)	125	0	0	100
PV4 (kW)	104	100	0	0	ESS1 (kW)	8	100	100	100
PV5 (kW)	110	0	100	0	ESS2 (kW)	32	100	100	100

for 24 h based on the MILP model and the NLP model are 130.49 kWh and 132.05 kWh, respectively, and the relative error is only 1.19%. Obviously, the optimization results based on the NLP model are local optimum rather than global optimum. By comparing the optimization results, it can be seen that the errors caused by linearization are acceptable. Moreover, the solution time of the MILP model is 12.81 s, and that of the NLP model is 2080 s, which indicates that the application of linearization technology in large networks has a more significant effect on improving computational efficiency.

In this section, two case studies are conducted on modified IEEE 34 and IEEE 123 test systems, respectively. The results indicate that the methods proposed in this paper have a good effect on the treatment of three-phase imbalance. According to the comparison of two cases, it can be seen that the three phase imbalance at each moment is mainly related to the loads distribution on three phases, but not to the total load at that time. However, the active power losses at each moment is positively correlate with the total loads at that time. According to the optimization results of two cases, more than 30% active power losses can be reduced by the methods proposed in this paper. Meanwhile, the regulation effect of current imbalance and maximum voltage imbalance in two cases also exist some differences. The current imbalance regulation effect in modified IEEE 34 system is better, while the voltage imbalance regulation effect in modified IEEE 123 system is better, which may be related to the size of the test system, the number of DGs and ESSs connected, and the number and location of TPLRDs installed. In addition, by comparing the calculation time, it can be found that the more nodes in the system, the longer the calculation time. Although the linearization method inevitably cause errors, it can significantly improve the computational efficiency, and the error analysis shows that the errors caused by the linearization methods used in the paper are acceptable. In short, in order to achieve the best three-phase unbalanced load regulation effect, it is necessary to comprehensively consider various factors, including the size of the network, the number of DGs and ESSs connected, the number and location of installed TPLRDs, etc. Meanwhile, the computational efficiency and the errors must be considered when solving the model.

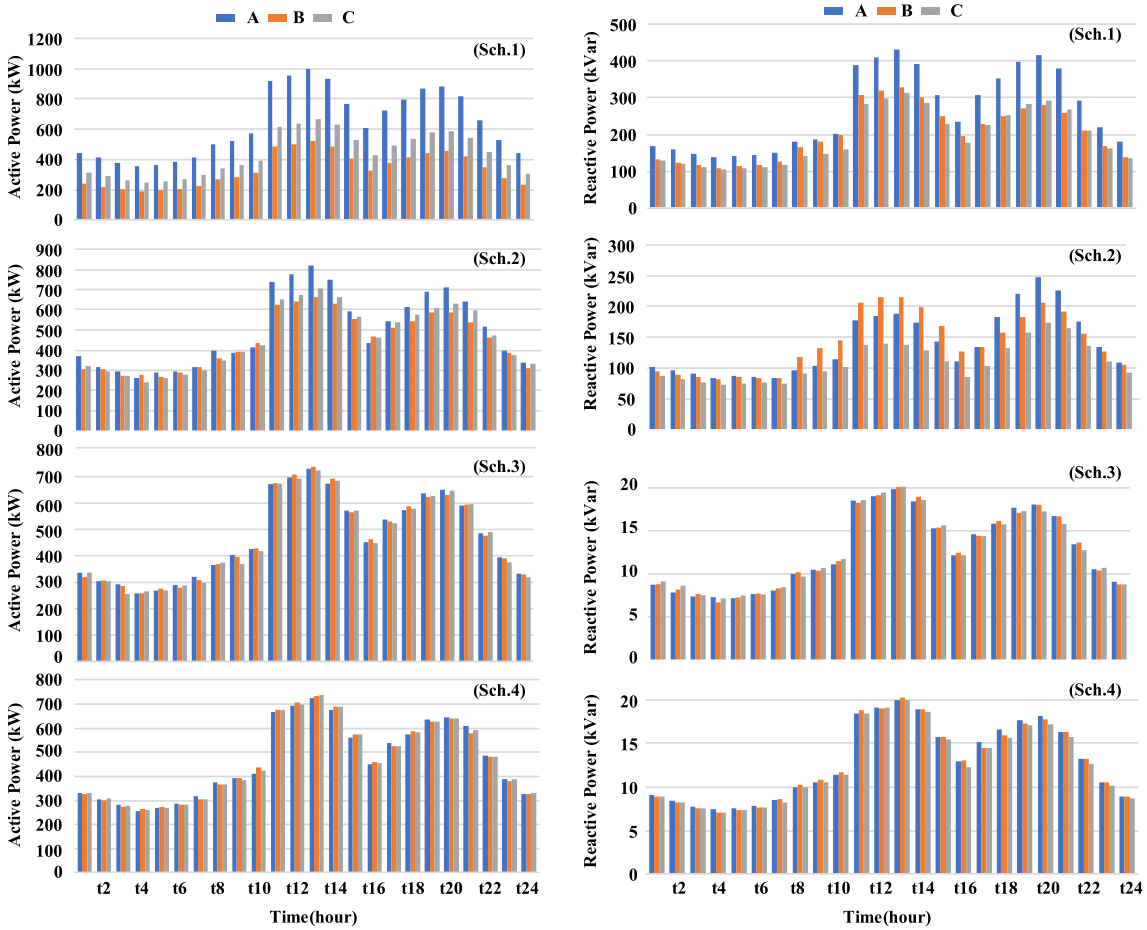

(a) Active power comparison (b) Reactive power comparison

Fig. 12. Hourly comparison of active /reactive power flowing through the transformer.

Table 8
Hourly active/reactive power imbalance (%) comparison for different schemes.

Time	Active power imbalance				Reactive power imbalance				Time	Active Power imbalance				Reactive Power imbalance			
	Sch.1	Sch.2	Sch.3	Sch.4	Sch.1	Sch.2	Sch.3	Sch.4		Sch.1	Sch.2	Sch.3	Sch.4	Sch.1	Sch.2	Sch.3	Sch.4
t1	46.7	17.9	5.22	1.61	23.5	14.1	4.21	2.21	t13	47.6	18.9	1.86	1.52	27.5	36.1	1.77	1.47
t2	46.9	5.98	1.04	3.17	23.9	14.4	9.04	2.38	t14	47.0	16.1	2.67	1.86	26.7	35.8	2.87	1.58
t3	46.5	8.11	8.51	3.44	24.6	14.6	3.88	2.34	t15	46.3	6.58	1.21	2.61	25.1	34.2	2.23	1.90
t4	46.8	13.4	2.95	3.34	24.1	14.3	8.29	5.34	t16	47.8	6.28	3.11	2.64	23.7	33.4	2.36	6.13
t5	46.4	9.57	2.86	1.34	22.9	13.1	3.92	2.67	t17	48.4	11.3	2.65	2.23	27.0	22.2	1.52	4.61
t6	46.1	5.65	3.51	3.52	22.1	11.1	1.57	2.56	t18	49.0	14.9	2.42	1.98	29.3	27.9	2.41	5.41
t7	45.8	5.91	7.22	4.56	22.4	10.8	4.64	3.51	t19	48.9	17	2.12	1.75	31.9	29.1	3.37	3.37
t8	45.1	12.4	2.53	2.72	22.5	23.7	5.23	2.92	t20	49.1	17.2	3.14	3.71	32.6	30.1	4.46	5.49
t9	45.8	1.78	8.54	2.45	21.6	28.2	4.64	2.78	t21	48.9	16.2	1.02	5.12	31.8	27.2	5.68	3.65
t10	47.6	5.58	2.42	6.52	21.6	31.0	5.25	2.56	t22	48.2	10.8	2.68	4.56	28.1	23.1	6.43	4.52
t11	47.7	15.6	0.78	1.15	26.9	33.9	1.74	2.12	t23	47.6	4.93	4.82	2.53	26.3	13.3	2.92	3.79
t12	47.9	17.4	2.19	1.36	27.4	35.5	2.08	0.52	t24	47.3	8.61	4.29	1.25	25.1	16.1	3.56	2.25

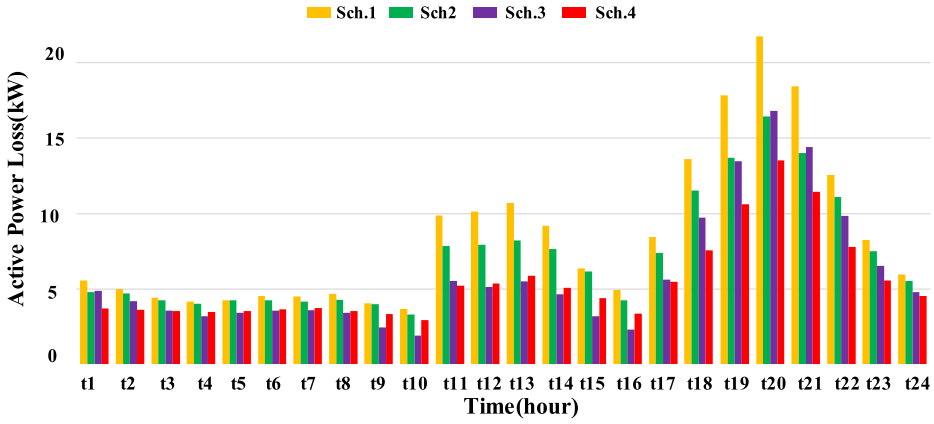

Fig. 13. Active power loss in DNS before and after installing TPLRD.

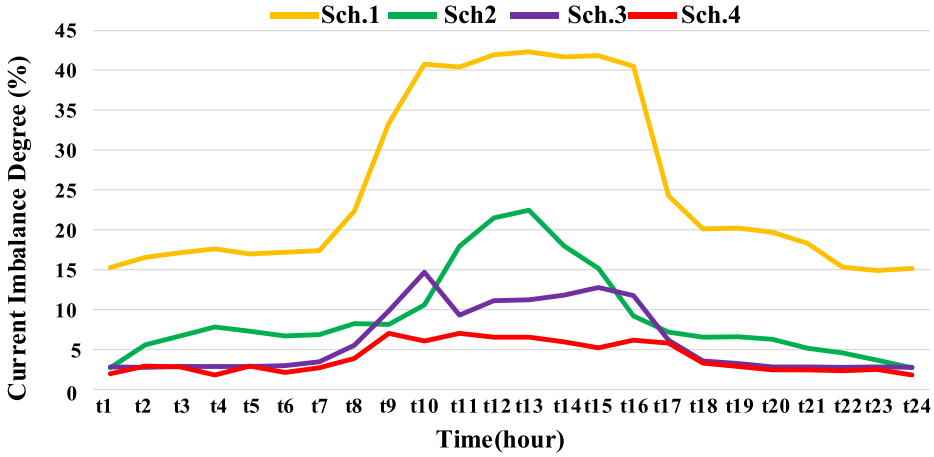

Fig. 14. Current Unbalance degree of root node before and after installed TPLRD.

7. Conclusion

In this paper, a new three-phase load-regulating device (TPLRD) is applied which consists of Y-connected and Δ-connected SVCs. Compared with current three-phase unbalanced load regulating device in the market, TPLRD is more cost-effective, which can adjust active and reactive loads simultaneously, and can also compensate the reactive power to improve the voltage waveform and power factor. Furthermore, a joint optimization model based on TPLRDs is proposed from the perspective of a whole system, the objective function is to minimize the total active power losses in DNSs, and the optimization goal is the operation of all TPLRDs in DNSs. Moreover, both the current and voltage imbalance degree are considered in the model simultaneously. Some linearization techniques are applied to convert the non-convex non-linear model to a MILP problem, which greatly improves the computational efficiency. Meanwhile, the errors caused by linearization are analyzed, and the results show that the errors are acceptable. It can be seen that our methods can achieve good results on three-

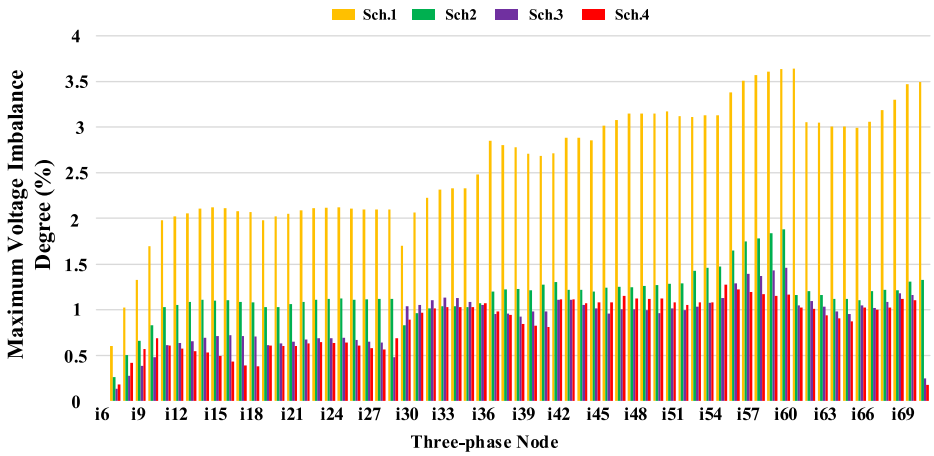

Fig. 15. Maximum voltage imbalance degree comparison of each node for 24 h.

Table 9
The comparison of hourly active power losses (kWh) in IEEE 123 test system.

Time period	t1	t2	t3	t4	t5	t6	t7	t8	t9	t10	t11	t12
NLP	3.615	3.456	3.434	3.456	3.356	3.551	3.635	3.534	3.029	3.029	5.207	5.197
MILP	3.695	3.596	3.512	3.466	3.514	3.631	3.721	3.511	3.305	2.914	5.195	5.349
Hourly error	2.23%	4.05%	2.26%	0.27%	4.69%	2.23%	2.37%	0.67%	3.6%	3.78%	0.22%	2.92%
Time period	t13	t14	t15	t16	t17	t18	t19	t20	t21	t22	t23	t24
NLP	5.849	4.821	4.196	3.213	5.763	7.829	11.183	14.22	11.82	8.276	5.846	4.373
MILP	5.857	5.055	4.362	3.345	5.474	7.553	10.60	13.53	11.44	7.786	5.534	4.531
Hourly error	0.13%	4.84%	3.95%	4.11%	5.01%	3.42%	5.18%	4.83%	3.17%	5.92%	5.33%	3.6%
MODEL	NLP		MILP		Total error		Calculation time		NLP		MILP	
Power losses	132.05 kWh		130.49 kWh		1.18%				2080 s		12.81 s	

phase imbalance regulation and has good scalability. It is not only helps to mitigate the three-phase imbalance in DNSs and reduce the active power losses, but also helps to improve the power quality of distribution networks and enhance the competitiveness of power companies. Furtherly, our methods provide the possibility for real-time dynamic adjustment of three-phase unbalanced loads in DNSs. For future researches, advanced models can be developed to solve the dynamic three-phase imbalance problem, considering the fluctuation of loads and the uncertainty of DG output. In addition, the optimal quantity and installation location of TPLRD, the coordination optimization between TPLRDs and ESSs are also worthy of further study.

Acknowledgments

This work was supported by the State Grid Corporation Headquarters of China and Economic & Technology Research Institute of State Grid Shandong Electric Power Company (52060018000X).

Appendix A

The original current imbalance degree constraint is (21), two ancillary variables S_1, S_2 are introduced:

$$\begin{aligned} S_1 &= s_{f,t}^a + \varepsilon^2 s_{f,t}^b + \varepsilon s_{f,t}^c \\ S_2 &= s_{f,t}^a + s_{f,t}^b + s_{f,t}^c \end{aligned}, \tag{25}$$

the expansion expression of the complex power S_1, S_2 are

$$|S_1| = \frac{1}{3}\,|P_a + P_b + P_c + \mathrm{j}(Q_a + Q_b + Q_c)|, \tag{26}$$

$$\begin{aligned} |S_2| &= \tfrac{1}{3}\left|P_a + \mathrm{j}Q_a + (-\tfrac{1}{2} - j\tfrac{\sqrt{3}}{2})(P_b + \mathrm{j}Q_b) + (-\tfrac{1}{2} + j\tfrac{\sqrt{3}}{2})(P_c + \mathrm{j}Q_c)\right| \\ &= \tfrac{1}{3}\left|\left(P_a - \tfrac{1}{2}P_b - \tfrac{1}{2}P_c + \tfrac{\sqrt{3}}{2}Q_b - \tfrac{\sqrt{3}}{2}Q_c\right) + \mathrm{j}\left(Q_a - \tfrac{1}{2}Q_b - \tfrac{1}{2}Q_c + \tfrac{\sqrt{3}}{2}P_c - \tfrac{\sqrt{3}}{2}P_b\right)\right| \end{aligned}, \tag{27}$$

and S_2 can be transformed as

$$|S_2| = \frac{1}{3}\begin{vmatrix} \frac{3}{2}P_a - \frac{1}{2}(P_a + P_b + P_c) + \frac{\sqrt{3}}{2}(Q_b - Q_c) \\ +j\frac{3}{2}Q_a - j\frac{1}{2}(Q_a + Q_b + Q_c) + j\frac{\sqrt{3}}{2}(P_c - P_b) \end{vmatrix}, \tag{28}$$

A parameter δ is defined to denote how far the output power of the transformer at each phase can deviate from the average of three-phase output

power.

If the following formulation hold

$$\begin{cases} -\frac{\delta}{2}(P_a + P_b + P_c) \leqslant \frac{3}{2}P_a \leqslant \frac{\delta}{2}(P_a + P_b + P_c) \\ -\frac{\delta}{2}(Q_a + Q_b + Q_c) \leqslant \frac{3}{2}Q_a \leqslant \frac{\delta}{2}(Q_a + Q_b + Q_c) \end{cases}, \tag{29}$$

the relationship below can be derived:

$$\begin{cases} -\frac{2\delta}{3}(P_a + P_b + P_c) \leqslant P_b - P_c \leqslant \frac{2\delta}{3}(P_a + P_b + P_c) \\ -\frac{2\delta}{3}(Q_a + Q_b + Q_c) \leqslant Q_b - Q_c \leqslant \frac{2\delta}{3}(Q_a + Q_b + Q_c) \end{cases}, \tag{30}$$

Next, substitute (29) and (30) into (28):

$$|S_2| \leqslant \frac{\delta}{3}\left|\begin{array}{l} \frac{1}{2}(P_a + P_b + P_c) + \frac{\sqrt{3}}{3}(Q_a + Q_b + Q_c) \\ +j\frac{1}{2}(Q_a + Q_b + Q_c) + j\frac{\sqrt{3}}{2}(P_a + P_b + P_c) \end{array}\right|, \tag{31}$$

Take the square to both sides:

$$\begin{aligned} |S_2|^2 &\leqslant \frac{\delta^2}{9}\left|\begin{array}{l} \frac{7}{12}(P_a + P_b + P_c)^2 + \frac{7}{12}(Q_a + Q_b + Q_c)^2 \\ +\frac{2\sqrt{3}}{2}(P_a + P_b + P_c)(Q_a + Q_b + Q_c) \end{array}\right| \\ &\leqslant \frac{\delta^2}{9} \times (\frac{7}{12} + \frac{\sqrt{3}}{3})((P_a + P_b + P_c)^2 + (Q_a + Q_b + Q_c)^2) \end{aligned}, \tag{32}$$

Meanwhile, take the square for both sides of (26):

$$|S_1|^2 = \frac{1}{9}((P_a + P_b + P)^2 + (Q_a + Q_b + Q_c)^2), \tag{33}$$

Dividing (32) by (33):

$$\left|\frac{S_2^2}{S_1^2}\right| \leqslant \delta^2 \times \left(\frac{7}{12} + \frac{\sqrt{3}}{3}\right), \tag{34}$$

The constraint (34) is equivalent to

$$CUF_{f,t} \leqslant \delta \times \sqrt{\left(\frac{7}{12} + \left(\frac{\sqrt{3}}{3}\right)\right)}, \tag{35}$$

Therefore, if (23) holds, the inequality constraint (35) holds.

Appendix B

The binary variable ρ can be replaced by a set of continuous constraints as below:

$$\rho - \frac{1}{2} = \rho_u - \rho_l, \tag{36}$$

$$\frac{1}{2} = \rho_u + \rho_l, \tag{37}$$

$$\rho_u\rho_l = 0, \quad \rho_u \geqslant 0, \quad \rho_l \geqslant 0\ , \tag{38}$$

where ρ_l and ρ_u are the auxiliary continuous variables associated with ρ. The constraint (37) ensures that either ρ_l or ρ_u is equal 1/2, and the complementary constraints (38) ensure that either ρ_l or ρ_u or both are zero. Consequently, the value of ρ can only is zero ($\rho_l = 0$, $\rho_u = 1/2$) or one ($\rho_l = 1/2$, $\rho_u = 0$).

References

[1] Singh M. Protection challenges under bulk penetration of renewable energy resources in power systems: a review. CSEE J Power Energy Syst 2017;3:365–79.

[2] Yong JY, Ramachandaramurthy VK, Tan KM, Mithulananthan N. A review on the state-of-the-art technologies of electric vehicle, its impacts and prospects. Renew Sustain Energy Rev 2015;49:365–85.

[3] Karimi M, Mokhlis H, Naidu K, Uddin S, Bakar AHA. Photovoltaic penetration issues and impacts in distribution network – a review. Renew Sustain Energy Rev 2016;53:594–605.

[4] Albadi AH, Elmoudi A, Metwally I, Alwahaibi A. Losses reduction in distribution transformers. Lect Notes Eng Comput Sci 2011;2189:873–6.

[5] Soltani SH, Rashidinejad M, Abdollahi A. Dynamic phase balancing in the smart distribution networks. Int J Electr Power Energy Syst 2017;93:374–83.

[6] Gnacinski P. Windings temperature and loss of life of an induction machine under voltage unbalance combined with over- or undervoltages. IEEE Trans Energy Convers 2008;23:363–71.

[7] San-Yi L, Chi-Jui W. On-line reactive power compensation schemes for unbalanced three phase four wire distribution feeders. IEEE Trans Power Delivery 1993;8:1958–65.

[8] Hooshmand RA, Soltani S. Fuzzy optimal phase balancing of radial and meshed distribution networks using BF-PSO algorithm. IEEE Trans Power Syst 2012;27:47–57.

[9] Zhai HF, Yang M, Chen B, Kang N. Dynamic reconfiguration of three-phase unbalanced distribution networks. Int J Electr Power Energy Syst 2018;99:1–10.

[10] Ding F, Loparo KA. Feeder reconfiguration for unbalanced distribution systems with distributed generation: a hierarchical decentralized approach. IEEE Trans Power Syst 2016;31:1633–42.

[11] Jabr RA, Singh R, Pal BC. Minimum loss network reconfiguration using mixed-integer convex programming. IEEE Trans Power Syst 2012;27:1106–15.

[12] Pegado R, Ñaupari Z, Molina Y, Castillo C. Radial distribution network reconfiguration for power losses reduction based on improved selective BPSO. Electr Power Syst Res 2019;169:206–13.

[13] Huijuan S, Chunhua P, Tingfang Y. A three-phase equilibrium reconfiguration strategy for distribution network. Power System Technology. 2014;38:789–94.
[14] Abbasi RS, Mehmood T. Feeder reconfiguration techniques: a review. International conference on energy systems and policies (ICESP). 2014. p. 1–5.
[15] Jinxiang Z, Mo-Yuen C, Fan Z. Phase balancing using mixed-integer programming [distribution feeders]. IEEE Trans Power Syst 1998;13:1487–92.
[16] Kaveh MR, Hooshmand RA, Madani SM. Simultaneous optimization of re-phasing, reconfiguration and DG placement in distribution networks using BF-SD algorithm. Appl Soft Comput 2018;62:1044–55.
[17] Hengfu F, Wanxing S, Jinli W, Ying L, Jinyu W, Siyuan W. Research on the method for real-time online control of three-phase unbalanced load in distribution area. Proc CSEE 2015;35:2185–93.
[18] Soltani S, Rashidinejad M, Abdollahi A. Stochastic multiobjective distribution systems phase balancing considering distributed energy resources. IEEE Syst J 2018;12:2866–77.
[19] Mostafa HA, El-Shatshat R, Salama MMA. Multi-objective optimization for the operation of an electric distribution system with a large number of single phase solar generators. IEEE Trans Smart Grid 2013;4:1038–47.
[20] Schweickardt G, Alvarez JMG, Casanova C. Metaheuristics approaches to solve combinatorial optimization problems in distribution power systems. An application to phase balancing in low voltage three-phase networks. Int J Electr Power Energy Syst 2016;76:1–10.
[21] Wang K, Skiena S, Robertazzi TG. Phase balancing algorithms. Electr Power Syst Res 2013;96:218–24.
[22] Sun S, Liang B, Dong M, Taylor JA. Phase balancing using energy storage in power grids under uncertainty. IEEE Trans Power Syst 2015;31:3891–903.
[23] Watson JD, Watson NR, Lestas I. Optimized dispatch of energy storage systems in unbalanced distribution networks. IEEE Trans Sustainable Energy 2018;9:939–50.
[24] Mateo V, Gole AM, Ho CNM. Design and implementation of laboratory scale static var compensator to demonstrate dynamic load balancing and power factor correction. IEEE electrical power and energy conference (EPEC). 2017. p. 1–6.
[25] Askarzadeh A. Capacitor placement in distribution systems for power loss reduction and voltage improvement: a new methodology. IET Gener Transm Distrib 2016;10:3631–8.
[26] Nejabatkhah F, Li YW. Flexible unbalanced compensation of three-phase distribution system using single-phase distributed generation inverters. IEEE Trans Smart Grid 2019;10:1845–57.
[27] Li P, Ji H, Wang C, Zhao J, Song G, Ding F, et al. Optimal operation of soft open points in active distribution networks under three-phase unbalanced conditions. IEEE Trans Smart Grid 2019;10:380–91.
[28] Weckx S, Driesen J. Load balancing with EV chargers and PV inverters in unbalanced distribution grids. IEEE Trans Sustainable Energy 2015;6:635–43.
[29] Chen B, Chen C, Wang J, Butler-Purry KL. Sequential service restoration for unbalanced distribution systems and microgrids. IEEE Trans Power Syst 2017;PP:1.
[30] Das S, Chatterjee D, Goswami SK. Tuned-TSC based SVC for reactive power compensation and harmonic reduction in unbalanced distribution system. IET Gener Transm Distrib. 2018;12:571–85.
[31] Association NEM. American national standard for electric power systems and equipment-voltage ratings (60 Hertz). National Electrical Manufacturers Association; 1996.
[32] IEEE recommended practice for monitoring electric power quality. IEEE Std 1159-2009 (Revision of IEEE Std 1159-1995) 2009:c1-81.
[33] Wang S, Chen S, Ge L, Wu L. Distributed generation hosting capacity evaluation for distribution systems considering the robust optimal operation of OLTC and SVC. IEEE Trans Sustainable Energy 2016;7:1111–23.
[34] Wang Z, Wang J, Chen C. A three-phase microgrid restoration model considering unbalanced operation of distributed generation. IEEE Trans Smart Grid 2018;9:3594–604.
[35] Ding T, Bo R, Gu W, Guo Q, Sun H. Absolute value constraint based method for interval optimization to SCED model. IEEE Trans Power Syst 2014;29:980–1.
[36] Davis M, Broadwater R, Hambrick J. Modeling and testing of unbalanced loading and voltage regulation. National Renewable Energy Laboratory; 2007.
[37] Rosenthal R. GAMS—a users' guide. Washington, DC: GAMS Development Corporation; 2017.